

Influence of grating characteristics on the operation of circular-grating distributed-feedback polymer lasers

G. A. Turnbull and A. Carleton

Organic Semiconductor Centre, and Ultrafast Photonics Collaboration, SUPA, School of Physics and Astronomy, University of St. Andrews, St. Andrews, Fife, KY16 9SS, United Kingdom

G. F. Barlow

School of Informatics, University of Wales, Bangor, Dean Street, Bangor, Gwynedd, LL57 1UT, United Kingdom

A. Tahraouhi and T. F. Krauss

Ultrafast Photonics Collaboration, SUPA, School of Physics and Astronomy, University of St. Andrews, St. Andrews, Fife, KY16 9SS, United Kingdom

K. A. Shore

School of Informatics, University of Wales, Bangor, Dean Street, Bangor, Gwynedd, LL57 1UT, United Kingdom

I. D. W. Samuel^{a)}

Organic Semiconductor Centre, and Ultrafast Photonics Collaboration, SUPA, School of Physics and Astronomy, University of St. Andrews, St. Andrews, Fife, KY16 9SS, United Kingdom

(Received 28 June 2004; accepted 26 April 2005; published online 25 July 2005)

We explore the influence of grating characteristics on the lasing performance of polymer circular-grating distributed-feedback lasers. A range of circular-grating sizes and profiles were fabricated on a single silica substrate, which was coated with a thin film of the conjugated polymer poly[2-methoxy-5-(2'ethylhexyloxy)-1,4-phenylene vinylene]. Variations in lasing threshold and surface-emitted slope efficiency were determined as a function of grating outer diameter and duty cycle. The experimental lasing results are compared with predictions from a theoretical analysis based on an adaptation of the transfer matrix method. We find that an outer diameter of at least 200 μm is required to minimize the threshold and optimize the surface-emitted slope efficiency. A groove-to-period duty cycle of $\sim 25\%$ gives the lowest lasing thresholds by optimizing the in-plane feedback. We also find that the structure of the polymer-air surface varies substantially with substrate duty cycle, which has implications for optimum device design. © 2005 American Institute of Physics. [DOI: 10.1063/1.1935131]

I. INTRODUCTION

In recent years, conjugated polymers have emerged as a promising new class of visible, solid-state laser gain media.^{1,2} Such polymers are semiconducting and have been applied as efficient light-emitting diodes.³ To date, however, only optically pumped polymer lasers have been successfully demonstrated, and there is considerable interest in achieving electrically pumped lasing, as a route to very broadly tuneable, visible diode lasers. A major challenge to this goal is that the lowest threshold excitation densities reported in optically pumped lasers are only marginally attainable using electrical excitation. There is much interest in further reducing laser thresholds through exploring novel resonator structures and improved optical designs. In particular, a better understanding of the photonic properties of such resonators⁴ should help towards this goal.

Distributed-feedback (DFB) lasers are a particularly promising resonator geometry for achieving low oscillation thresholds in a configuration that can also emit a narrow

linewidth and a well-defined output beam. One recent area of interest has been the study of DFB resonators that apply feedback in more than one direction in the organic semiconductor waveguide.⁴⁻¹² These include egg-box bigrating structures,⁴⁻⁸ in which feedback is applied in two orthogonal directions, and hexagonal photonic crystal structures,^{9,10} in which feedback is applied in three directions. These two-dimensional structures can significantly improve the operating characteristics of surface-emitting DFB lasers, compared with conventional one-dimensional (1D) gratings.⁵⁻⁷ They can lead to lower lasing thresholds, improved slope efficiencies, and near-diffraction-limited output beams. The mechanisms by which these gratings control light emission and propagation have been explored by relating the emission properties of the laser with the photonic-mode dispersion of the device.⁴

A natural extension of these basic two-dimensional (2D) structures would be to apply feedback in *all* directions in the plane. This is possible using circular DFB (CDFB) gratings as proposed by Erdogan and Hall¹³ and demonstrated with a GaInAsP/InP gain medium by Wu *et al.*¹⁴ A semiconducting polymer CDFB laser was also recently demonstrated by Bauer *et al.*,¹¹ who have observed visible lasing following

^{a)}Author to whom correspondence should be addressed; electronic mail: idws@st-and.ac.uk

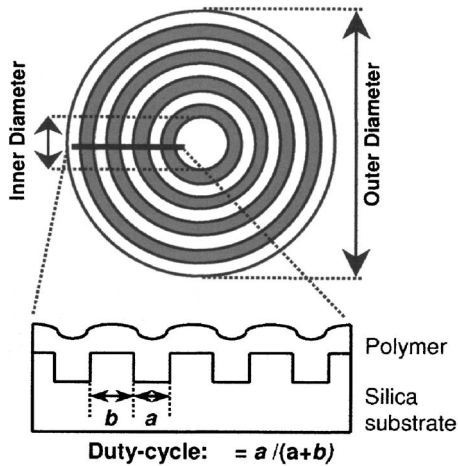


FIG. 1. The generic structure of the CDFB lasers: (a) schematic plan view and (b) schematic cross section through laser structure.

both one-photon¹¹ and two-photon absorption.¹² While the other 2D gratings are usually produced holographically, the CDFB structures are defined using electron-beam lithography. This is a more complicated processing technique, but offers much greater flexibility in the design and can allow parameters such as grating profile and length to be systematically varied. Such parameters are likely to have a significant influence on the operation of the laser; though these have not been studied in detail for conjugated polymers with any DFB resonator. In this paper, we explore the influence of the grating size and shape in CDFB polymer lasers, both to understand the device physics and identify an optimum resonator design. We study a range of grating profiles and sizes, and compare experimental lasing results with predictions from a theoretical model. In doing so, we obtain new insight into the practical design criteria for low-threshold polymer lasers.

II. EXPERIMENTAL AND THEORETICAL METHODS

A. General methodology—Choice of design parameters

The generic structure of the CDFB lasers is shown schematically in Fig. 1. It consists of a semiconducting conjugated polymer film deposited on a corrugated silica substrate. The silica–polymer–air structure forms an asymmetric slab waveguide, designed only to support the lowest-order transverse electric mode within the emission band of the polymer. The corrugated grating comprises a set of concentric circular grooves. These are designed to have a radially periodic, square-wave structure of period Λ , depth d , and duty cycle—or groove width to period ratio— Γ . Individual gratings were further defined by a given outer diameter of the largest concentric ring, and an inner diameter defined by the width of the inner cylindrical peak. For a given period and depth of the grating, the duty cycle and inner and outer grating diameters constitute independent design parameters, which can be readily adjusted to optimize performance. In this work, we present an investigation of the effect on laser performance of two of these parameters, the outer diameter and duty cycle. While these are studied directly in the con-

text of CDFB lasers, many of our results are more widely applicable to other one- and two-dimensional DFB resonators.

B. Fabrication of laser structures and experimental configuration

To carry out these experiments, two sets of gratings were defined in the fused-silica substrate, each with a radial period of 400 nm. In the first set, the inner diameter and duty cycle were fixed at 300 nm and 25%, while the outer diameter was varied between 50 and 300 μm . In the second set, the inner and outer diameters were fixed at 300 nm and 100 μm , while the duty cycle was varied between 20% and 70%. These grating patterns were defined initially by electron-beam lithography on a Leica EBPG-5 Beamwriter at the University of Glasgow, using a poly(methyl-methacrylate) resist layer coated on top of the silica substrate. A thin film of NiCr (30 nm) was used as a charge-dissipation layer and removed prior to development using chrome etch. The pattern was subsequently transferred into the substrate via reactive ion etching using fluorine chemistry (CHF_3). All of the gratings had a radial period of 400 nm and a depth of 125 ± 10 nm. The corrugations in the structure provided both distributed feedback and output coupling of the guided optical mode via second- and first-order Bragg scattering.

To complete the laser structures, a thin film of poly[2-methoxy-5-(2'-ethylhexyloxy)-1,4-phenylene vinylene] (MEH-PPV) was spin coated from solution in chlorobenzene (5-mg MEH-PPV in 1-ml chlorobenzene; spin speed of 1200 rpm) onto the silica substrate. This formed a polymer layer with an average thickness of ~ 100 nm as measured on an untextured region of the substrate using a DekTak-3 surface profiler.

Immediately after fabrication, the sample was transferred to a vacuum chamber in which it was held under a vacuum of $\sim 10^{-4}$ mbar during the subsequent optical characterization. For the lasing measurements, the sample was excited at 532 nm by the second harmonic of a Nd:YVO₄ microchip laser that generated pulses of 1-ns duration at 5-kHz repetition rate. The pump-laser output energy was varied using neutral density filters, and then focussed onto the sample to a circular spot of ~ 150 - μm diameter. Output energies from the laser were measured using a calibrated silicon energy meter for a range of excitation powers. The spectral output from the laser in an angular range $\pm 5^\circ$ around normal incidence was measured using a fiber-coupled charge-coupled device (CCD) spectrometer.

C. Theoretical analysis of CDFB structures

The theoretical analysis of polymer CDFB lasers has been described in detail elsewhere,^{13,15–18} and so in this section we only briefly outline the analytical approach used here to calculate the curves in Figs. 6 and 7. The theoretical analysis begins with the assumption that the field in the device can be separated into transverse, radial, and azimuthal harmonic components.¹⁶ An adaptation of the transfer matrix method (TMM) is used, with appropriate boundary conditions, to derive an eigenfunction representing the dispersion

relation of the slab waveguide. By definition, the dispersion relation has roots corresponding to the transverse electric (TE) modes supported by the polymer waveguide. An argument principle algorithm is then used to locate the eigenvalues without the need for initial guesses.¹⁷ The eigenvalues directly allow the calculation of transverse field profiles. The strong pump absorption ($\sim 10^5 \text{ cm}^{-1}$) and the resulting non-uniform gain profile in the polymer are included in the TE analysis for the calculation of mode-confinement factors.

Refractive indices of 1.9 and 1.46 are used for the polymer and substrate layers, corresponding to the peak-gain wavelength in MEH-PPV of 620 nm. Calculating the supported TE modes over a range of polymer film thicknesses, an optimum confinement of 22% for the fundamental TE mode occurs when the guide layer is 150-nm thick. For the thickness of 100 nm used in the experimental devices, the confinement factor is calculated to be 18%. These values are lower than would otherwise be the case for a waveguide with a uniform gain profile. Indeed, we find that the confinement significantly reduces with increasing film thickness beyond 150 nm, because of a reduced overlap between the nonuniform gain profile and the optical field.

Once the TE confinement factor and field profile have been calculated, the effect of the grating profile must be considered. In a circularly symmetric grating, a steady-state field is assumed to oscillate harmonically in the azimuthal and radial coordinates of the structure. The azimuthal-mode dependence is first removed by an expansion of the cylindrical field into its harmonic Fourier components. This leaves only the radial propagating component to define the modes of the laser during steady-state operation.

By applying an appropriate refractive-index perturbation to the wave equation describing the radial propagation of the field, a set of coupled partial differential equations are derived that describe the amplitude changes in the optical field.¹⁶ In the case of first-order gratings, two coupled equations are obtained representing inward and outwardly propagating radial waves. For second-order gratings, an additional third equation results from the analysis, describing the coupling of the confined field to a vertically propagating radiation mode. The coupled field equations are finally converted into a matrix form relating the amplitudes of the inward and outwardly propagating waves between two points along the radius of the structure. For the polymer CDFB, the index perturbation is assumed to arise from the 400-nm-period square grating etched into the glass substrate prior to the deposition of the polymer. The experimental gratings are designed to have a tooth height of 120 nm. In the analysis we also include a 60-nm modulation depth at the polymer-air interface to account for the residual corrugation on this surface, commonly found in spin-coated polymer DFB lasers.^{19,20}

Under steady-state operation, the radial field must be evanescent at the outer circumference of the structure, while remaining finite at the center. This unique boundary condition for circular DFB lasers is applied to the matrix product to give an eigenfunction for the laser cavity modes, in a similar manner to the calculation of the TE modes discussed previously. The roots of the eigenfunction, once found, yield

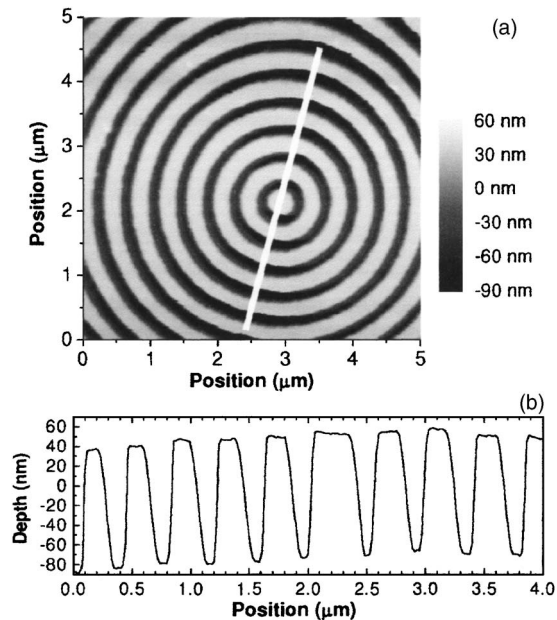


FIG. 2. (a) Atomic force microscope image of the center of a CDFB substrate grating. (b) Cross section of the substrate grating profile along the white line in (a).

the detuning and threshold gain of each mode. The values of threshold gain shown in Figs. 5 and 6 represent the net gains required to exceed only the Bragg-reflectivity losses in the waveguide. Other losses such as absorption and random scattering are not explicitly included in the calculation, but would need to be overcome in achieving a net threshold gain.

III. RESULTS

A. Laser structures

Figure 2 shows the structure of a typical circular DFB grating. Figure 2(a) shows an atomic force microscope image of a $5 \times 5\text{-}\mu\text{m}^2$ region located near the center of the circular grating. The grating was designed to have a period of 400 nm, a duty cycle of 40%, and a central ring diameter of 300 nm. The figure shows that a very uniform circular structure can easily be fabricated in the silica substrate. The exact profile of the grating is shown more clearly in Fig. 2(b), which shows a cross section through the center of the grating on the substrate. The depth of the grating is 125 ± 10 nm. We find that the grating differs from the ideal square-walled shape, and hence slightly changes the effective duty cycle from the intended value.

Figure 3(a) shows an atomic force microscope profile of the polymer-air interface on the same grating. It is clear that this surface has the same periodicity of 400 nm, however, the depth of the grating is significantly reduced compared with the substrate. This reduced grating depth on the top of the polymer film is commonly found when spin coating polymer layers on top of corrugated substrates.^{19,20} The difference in grating depths on the two surfaces mean that the polymer film is modulated in thickness by ~ 80 nm. We find here that this reduction in the top-surface grating depth changes substantially with the duty cycle of the substrate corrugation. Figure 3(b) illustrates this with measurements of corrugation

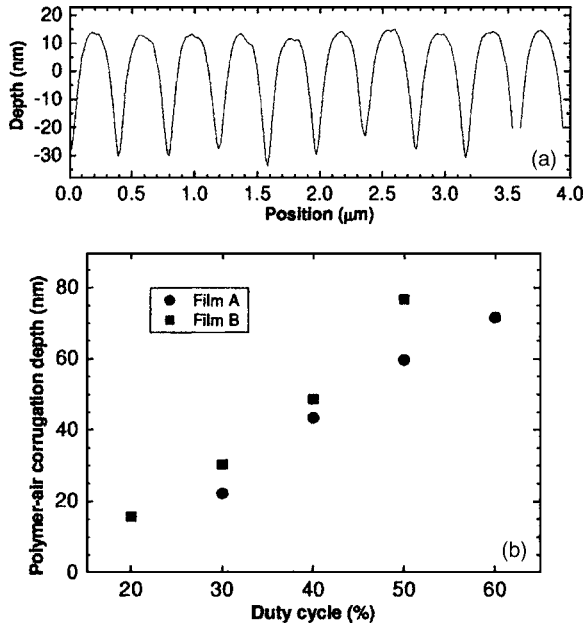


FIG. 3. (a) Radial profile of the polymer-air interface, measured for the same substrate grating as Fig. 2 (N.B. Profile does not include the center ring of the grating). (b) Corrugation depths on the polymer-air interface for a range of grating duty cycles.

depths on the polymer-air interface for a range of duty cycles. Two data sets are presented (A, B), each for a single polymer film deposited on a common substrate (grating depth: 125 nm). The thickness of the polymer films was measured on a nontextured region of the substrate, and was found to be approximately 100-nm thick. It is clear that the corrugation depth of the polymer-air surface increases significantly with duty cycle. The depth of top-surface corrugations ranges between $\sim 10\%$ and 60% of the substrate grating depth.

B. Power and spectral characteristics

Figures 4 and 5 illustrate the typical power and spectral characteristics of the CDFB lasers studied. Figure 4 shows the input-output characteristic of a laser of 250- μm outer diameter. The laser had a threshold of 19 nJ and an energy slope efficiency of 0.13%. This threshold is approximately five times larger, and slope efficiency is significantly lower, than that observed with MEH-PPV DFB lasers using holo-

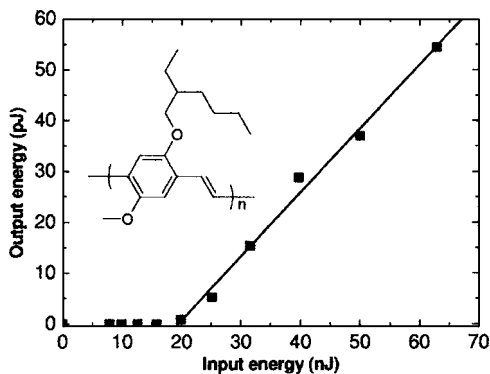


FIG. 4. Typical power characteristics of a polymer CDFB laser. Inset shows the chemical structure of MEH-PPV.

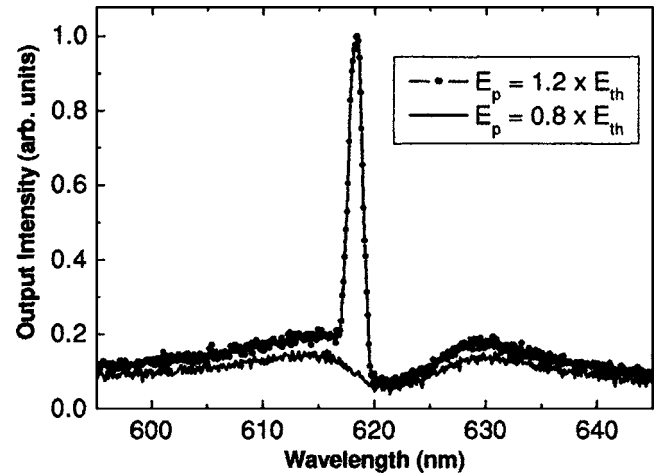


FIG. 5. Spectral characteristics of a typical polymer CDFB laser when pumped 20% above and 20% below lasing threshold.

graphically defined bigrating feedback structures.⁸ We attribute these differences to both the shorter grating length used here and the different grating profiles, which are designed to minimize the surface output-coupling losses.

Figure 5 shows the spectrum of emission collected over a small angular range ($\sim \pm 5^\circ$) around the normal to the plane of the waveguide. The solid line shows the emission when pumping 20% below the laser threshold. Two peaks dominate this spectrum at wavelengths of 615 and 630 nm. These arise from light that is initially emitted into the TE_0 waveguide mode, and then subsequently Bragg scattered out of the guide. The dip at 621 nm corresponds to a photonic stop band in which the emission is reduced.⁴ The dashed line in the figure shows the emission spectrum when pumping 20% above the laser threshold. The laser emission is stimulated to emit in a mode at 618 nm, near one edge of the stop band. Similar band-edge lasing has previously been observed in other polymer DFB lasers.^{4,8,11} This narrow peak, of around 1-nm linewidth, limited by the spectrometer resolution, rapidly grows with pump energy to dominate the spectrum.

C. Threshold dependence on the grating outer diameter and duty cycle

Figure 6 shows the dependence of CDFB lasing threshold on the outer diameter of the gratings. The points on the graph represent the experimental data for CDFB gratings of diameters between 50 and 300 μm . Measurements were taken for two polymer films deposited on the same substrate under similar conditions. These two sets of data are shown to indicate the film-to-film variability in threshold. We find that the measured thresholds drop by a factor of three as one increases the outer diameter from 50 to 200 μm . Above 200 μm the threshold becomes relatively insensitive to further increases in diameter.

The full line in the figure shows the calculated behavior of the threshold-gain coefficient. Assuming that the focusing of the excitation beam remains constant, one would expect the threshold-gain parameter to be directly proportional to the pump pulse energy at the lasing threshold. The experi-

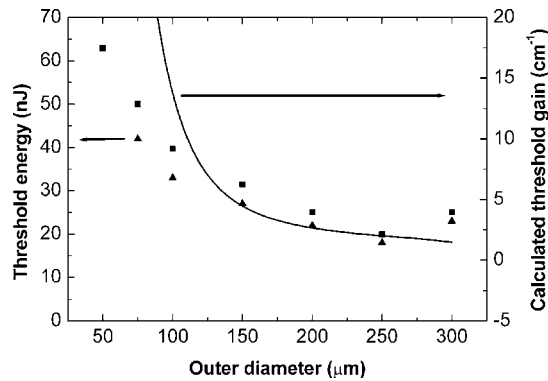


FIG. 6. Experimentally measured threshold energy (points) and calculated threshold gain (line) as a function of the grating outer diameter. The triangles and squares represent the data for different polymer films.

mental data and theory should therefore exhibit the same functional dependence on the grating outer diameter. We find that the variation in threshold gain is qualitatively similar to the experimental data, with a rapid change for grating diameters below $150\ \mu\text{m}$, and only a slow decrease above $200\ \mu\text{m}$. The analysis, however, predicts a significantly greater relative change in threshold over the $50\text{--}300\text{-}\mu\text{m}$ range than is observed experimentally.

We also observed that the slope efficiencies of the lasers increase significantly with increasing diameter. Indeed, lasers with outer diameters above $200\ \mu\text{m}$ exhibit output efficiencies as much as ten times higher than the smallest CDFB lasers. This suggests that for small diameters much of the laser output is emitted radially into the surrounding slab waveguide.

The dependence of laser threshold on the grating duty cycle is shown in Fig. 7. The groove-to-period duty cycle was varied between 20% and 70%. Again, several sets of data are shown to indicate the film-to-film variability in the threshold measurements. We find that changes to the grating profile can have a large effect on the lasing threshold, which changes between 21 and 305 nJ over the range of structures studied. Thresholds are low for small duty cycles $\sim 25\%$, and reach a maximum around a duty cycle of 50%. At still larger duty cycles, the lasing threshold again falls. The data is asymmetric about the 50% point, with the lowest thresholds

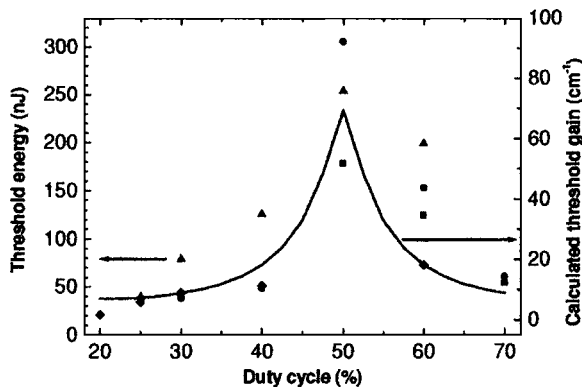


FIG. 7. Experimentally measured threshold energy (points) and calculated threshold gain (line) as a function of the grating duty cycle. The triangles, circles, diamonds, and squares represent the data for different polymer films.

observed around 25%. While the repeatability of threshold data was good for the lowest and highest duty cycles, we found that there was considerable variation for duty cycles of 40%, 50%, and 60%.

The full trace in the figure shows the dependence of threshold gain on duty cycle, as predicted from the analysis. The curve is roughly symmetrical about 50% duty cycle and shows a sharp peak at this value. The calculated threshold gains vary by a factor of ten over the range of duty cycles studied.

We have also observed that the slope efficiencies of the lasers are highest at low duty cycles and significantly drop for duty cycles around 50%. Indeed the output from the 50% duty-cycle laser is dominated by Bragg-scattered spontaneous emission, even when pumping well above the laser threshold. It suggests that for 50% duty cycle, the first-order scattering is sufficiently strong to compete effectively with the build up of stimulated emission.

IV. DISCUSSION

The results from the previous section represent a systematic study of the design parameters of grating structures in polymer CDFB lasers. Overall, we find broad agreement between the experimental results and the theoretical predictions. In this section we critically compare the two and draw conclusions for the optimum design parameters for polymer CDFB lasers. It is worth emphasizing that the gratings fabricated for this study differ slightly from the modeled square-profile structures, but represent structures that can be realistically produced, and are still useful for drawing conclusions about the optimized design of these devices.

We will first consider the variation of threshold with the grating outer diameter, and subsequently consider the dependence on duty cycle. In the case of the outer-diameter experiment, we find that the threshold drops with increasing diameter, and that both the theory and experimental data show a similar trend. There is a rapid change in threshold for diameters below $150\ \mu\text{m}$, and above outer diameters of $200\ \mu\text{m}$ there is only a modest further drop in threshold. This represents a useful general result in the context of organic semiconductor DFB lasers, since most other resonators studied to date have made use of long gratings of dimensions $>1\ \text{cm}$. The data in Fig. 6, however, provides a clear idea of the feedback length required in a polymer DFB laser in order to minimize threshold.

Naturally, the feedback length is strongly dependent on both the depth of the corrugation and the difference in refractive index between the polymer and substrate layers. In each respect, the structures studied here are typical of the parameters used in the literature. Many conjugated polymers, including derivatives of poly(phenylene-vinylene) and poly(fluorene), have an in-plane refractive index of around 1.9 at the peak of the material gain [although ladder-type poly(paraphenylene) has a lower refractive index]. Frequently, polymer DFB lasers have used feedback gratings of depths similar to the polymer film thickness in order to maximize feedback. Typically, polymer films of thicknesses around 100

nm are used to give high absorption at the pump wavelength combined with single transverse-mode waveguiding of the laser light.

Considering the data in Fig. 6 in more detail, we find that the calculated relationship of threshold gain to outer diameter differs from that of the experimental threshold pump energies. The experimental data show a smaller relative change in threshold across the parameter space investigated. There are several possible explanations for this disparity. We recall that the values of threshold gain represent the *net gains* required to exceed only the Bragg-reflectivity losses in the waveguide. Other (parasitic) losses are not explicitly included in the calculation, but would first need to be surmounted via optical pumping to achieve a positive net gain. The offset between the zero levels of the theory and experimental data suggests that in the fabricated waveguides, there may be significant parasitic losses. These would include both absorption and random scattering, which must be overcome to achieve transparency in the waveguide. An additional explanation for the disparity may be that the perturbation analysis used here is not completely adequate for such strongly modulated waveguides. For example, the inherent assumption that the electric field is unchanged between the groove and peak of the grating is unlikely to be valid. This could lead to TE-TM cross coupling, where the polymer layer is thickest, that might significantly modify lasing thresholds from those predicted by the analysis.

The values of threshold energy measured for these CDFB lasers are comparable with other CDFB threshold data in the literature,¹¹ though are higher than the thresholds obtained with “egg-box” bigrating feedback.^{4–8} One might anticipate that, when feedback is applied in *all* directions in the plane of the guide using CDFB structures, a lower lasing threshold would result. Current data suggest that this is not the case. We believe that a reason for higher lasing thresholds may be related to a poor spatial overlap of the very strongly localized radial mode with the optically pumped region of the waveguide. This hypothesis is the subject of ongoing studies.

We next consider the dependence of the laser threshold on the duty cycle of the grating, as shown in Fig. 7. Significantly, we find that the grating shape can have a very large impact on the laser operation, and so represents an important design parameter that has been largely overlooked in the polymer laser literature. From our analysis, we can identify the large increase in threshold at 50% duty cycle to result from the combined effect of a minimum in the in-plane feedback and a maximum in surface-output coupling. For an ideal square-wave grating, the in-plane feedback should drop to zero at 50% duty cycle.¹⁸ Our experimental gratings are not ideal square waves (particularly on the polymer–air interface), which means that they provide some weak feedback, even at the nominal 50% duty cycle.

Overall, we found a close correlation between the experimentally measured threshold powers and the calculated values of threshold gain from the analysis. One noticeable disparity is that while the theory suggests a symmetrical variation in threshold about 50% duty cycle, experimentally

we found an asymmetry in the data, with the thresholds at high duty cycles greater than those at low duty cycles.

To understand the asymmetry in the data, we must reconsider the graph in Fig. 3, which shows the change in the corrugation depth of the top surface of the polymer film as a function of duty cycle. As the duty cycle increases, the corrugation on the polymer–air interface becomes significantly deeper, as a result of the spin-coating deposition process. Thus the overall shape of the waveguide varies significantly with changing duty cycle. One consequence of having a second strongly modulated interface of the same period and phase as the substrate–polymer corrugation is to partly cancel the coupling coefficient of the grating, and hence reduce the feedback coupling strength. One may understand this simply by noting that the coupling coefficient arises from a periodic modulation of the effective waveguide index via a modulation of the thickness of the polymer-guide layer. If the polymer is corrugated on one interface, but flat on the other interface, then there will be a strong modulation of the effective guide index. If, however, the polymer has a similar corrugation on each interface, then the guide index at any point along the waveguide will remain approximately constant. The result of this effect is that the stronger modulation of the polymer–air interface at large duty cycles leads to a lower coupling of the counter-propagating waveguide modes, a weaker feedback, and hence higher lasing thresholds.

The significant variations in threshold energies for duty cycles between 40% and 60% may also be due to the fabrication techniques employed. For this range of duty cycles, we find, from the analysis, that the threshold gain is very sensitive to small changes in the grating profile. In a previous work we have shown that feedback coupling tends to zero at 50% duty cycle.¹⁶ It is also evident from Fig. 3(b) that there can be some film-to-film variation in the corrugation of the polymer–air interface. One might, therefore, infer that small changes in the polymer deposition may lead to large relative variations in the lasing threshold within this limited parameter space. In contrast, for duty cycles in the range 20%–40%, the threshold is relatively insensitive to the grating profile, and so variations in the waveguide fabrication will have much less impact on the laser operation.

V. CONCLUSIONS

From the preceding discussion we may now summarize the design features that will lead to a minimum oscillation threshold in surface-emitting polymer CDFB lasers. In doing so it is important to take into account practical fabrication issues, in addition to guidance from the theoretical analysis.

For a substrate–polymer step in a refractive index of ~ 0.4 (typical in organic semiconductor lasers) and a grating of ~ 100 -nm deep, both the analysis and the experimental data suggest that one should use an outer diameter of at least $200\ \mu\text{m}$. Since fabrication using electron-beam lithography, at high spatial resolution, is limited practically to small writing areas, a circular grating of 200 – 250 - μm diameter would be most realistic. For a second-order grating, the analysis suggests that the groove-to-period duty cycle should either be $\sim 25\%$ or $\sim 75\%$. From a practical point of view, taking

account of the spin-coating deposition of the polymer waveguide layer, it is clear that one should choose the shorter of the two to minimize any reduction in the coupling coefficient from a corrugation on the top surface of the polymer film. Alternatively, one may employ a different fabrication procedure, which might ensure that the polymer film had a grating on only one side. One such procedure is solvent-assisted micromoulding, which has been successfully applied to polymer lasers.²¹ In this technique the polymer is initially deposited onto a flat substrate, and is subsequently patterned on the top surface using an appropriate mould. Such a procedure automatically makes one surface of the polymer layer flat, meaning that the 75% duty cycle may be equally appropriate for low thresholds.

Although the current study has focused on the device physics of CDFB polymer lasers, many of our findings should be more widely applicable to other polymer DFB structures. The effect of duty cycle on feedback, for example, is anticipated to be similar for lasers with linear gratings. The substantial change of the top-surface structure with grating shape is particularly important to the strength of the feedback, and potentially, the photonic dispersion of the device.²² While the threshold energies measured in this work are higher than those reported for bigrating structures,¹¹ we anticipate that more sophisticated circular grating structures should lead to lower thresholds.¹⁸ Additionally, the circular grating geometry may offer several interesting device configurations. These include the fabrication of isotropic edge-emitting lasers, arrays of surface-emitting lasers with circular beam profiles, and the possibility of controlling output-beam focusing through chirping the gratings of individual resonators.

We should finally note that there is one other parameter of the CDFB structures that has not been explored in the current study; that is, the central ring diameter of the grating. By varying the inner ring diameter, one may introduce an effective phase shift in the feedback. Quarter-wave-shifted DFB structures are commonly used in first-order, linear DFB lasers in order to achieve single-frequency operation. This is generally not necessary in second-order DFB structures in which surface-emitting output-coupling losses at the two band edges tend to differ in magnitude, giving a robust frequency selection mechanism of one band edge over the other. Nonetheless, it has been shown theoretically that the frequency of the lasing mode in CDFB lasers may be tuned across the stop band, and this can result in a lower lasing threshold.¹⁶ This effect has been explored in a recent experimental study.²³

To conclude, we have explored the design parameters of CDFB surface-emitting polymer lasers, with the aims of un-

derstanding the physics of the devices and finding an optimized resonator design for low-threshold operation. We have found, for typical polymer laser structures used in the literature, that the optimum grating diameter is around 200 μm , while the optimum duty cycle is 25%. We find that the practical considerations in the fabrication of these lasers are important in optimizing the design of the structures. While our current study has focused on CDFB structures, the results should be more generally applicable to other 1D and 2D polymer DFB lasers.

ACKNOWLEDGMENTS

The authors gratefully acknowledge the technical support of the Nanoelectronics Research Centre at the University of Glasgow. We are grateful to the EPSRC and SHEFC, for financial support, and Covion for the supply of the polymer.

- ¹N. Tessler, *Adv. Mater. (Weinheim, Ger.)* **11**, 363 (1999).
- ²M. D. McGehee and A. J. Heeger, *Adv. Mater. (Weinheim, Ger.)* **12**, 1655 (2000).
- ³R. H. Friend *et al.*, *Nature (London)* **397**, 121 (1999).
- ⁴G. A. Turnbull, P. Andrew, W. L. Barnes, and I. D. W. Samuel, *Phys. Rev. B* **67**, 165107 (2003).
- ⁵S. Riechel, C. Kallinger, U. Lemmer, J. Feldmann, K. Gombert, V. Wittwer, and U. Scherf, *Appl. Phys. Lett.* **77**, 2310 (2000).
- ⁶G. Heliotis, R. Xia, G. A. Turnbull, P. Andrew, W. L. Barnes, I. D. W. Samuel, and D. D. C. Bradley, *Adv. Funct. Mater.* **14**, 91 (2004).
- ⁷J. Stehr *et al.*, *Adv. Mater. (Weinheim, Ger.)* **15**, 1726 (2003).
- ⁸G. A. Turnbull, P. Andrew, W. L. Barnes, and I. D. W. Samuel, *Appl. Phys. Lett.* **82**, 313 (2003).
- ⁹M. Meier, A. Mekis, A. Dodabalapur, A. Timko, R. E. Slusher, J. D. Joannopoulos, and O. Nalamasu, *Appl. Phys. Lett.* **74**, 7 (1999).
- ¹⁰A. Yokoo, M. Notomi, H. Suzuki, M. Nakao, T. Tamamura, and H. Masuda, *IEEE J. Quantum Electron.* **QE-38**, 938 (2002).
- ¹¹C. Bauer, H. Giessen, B. Schnabel, E. B. Kley, C. Schmitt, U. Scherf, and R. F. Mahrt, *Adv. Mater. (Weinheim, Ger.)* **13**, 1161 (2001).
- ¹²C. Bauer, B. Schnabel, E. B. Kley, U. Scherf, H. Giessen, and R. F. Mahrt, *Adv. Mater. (Weinheim, Ger.)* **14**, 673 (2002).
- ¹³T. Erdogan and D. G. Hall, *J. Appl. Phys.* **68**, 1435 (1990).
- ¹⁴C. Wu, M. Svilans, M. Fallahi, T. Makino, J. Glinski, C. Maritan, and C. Blaauw, *Electron. Lett.* **27**, 1819 (1991).
- ¹⁵C. Wu, T. Makino, J. Glinski, R. Maciejko, and S. I. Najafi, *J. Lightwave Technol.* **9**, 1264 (1991).
- ¹⁶G. F. Barlow and K. A. Shore, *IEE Proc.: Optoelectron.* **148**, 165 (2001).
- ¹⁷G. F. Barlow and K. A. Shore, *Int. J. Numer. Model.* **14**, 291 (2001).
- ¹⁸G. F. Barlow, K. A. Shore, G. A. Turnbull, and I. D. W. Samuel, *J. Opt. Soc. Am. B* **21**, 2142 (2004).
- ¹⁹S. Riechel, U. Lemmer, J. Feldmann, T. Benstem, W. Kowalsky, U. Scherf, A. Gombert, and V. Wittwer, *Appl. Phys. B* **B71**, 897 (2000).
- ²⁰P. Andrew, G. A. Turnbull, I. D. W. Samuel, and W. L. Barnes, *Appl. Phys. Lett.* **81**, 954 (2002).
- ²¹J. R. Lawrence, G. A. Turnbull, and I. D. W. Samuel, *Appl. Phys. Lett.* **82**, 4023 (2003).
- ²²M. G. Salt, P. Andrew, and W. L. Barnes, *J. Opt. Soc. Am. B* **18**, 240 (2001).
- ²³A. Jebali, R. F. Mahrt, N. Moll, E. Erni, C. Bauer, G. L. Bona, and W. Bächtold, *J. Appl. Phys.* **96**, 3043 (2004).